Article

Selection and Optimization Design of PDC Bits Based on FEM Analysis for Drilling Long Horizontal Sections of Shale Formations

Lulin Kong [1,*], Zhaowei Wang [2,*], Haige Wang [3], Mingyue Cui [1], Chong Liang [1], Xiangwen Kong [1] and Ping Wang [1]

[1]   Research Institute of Petroleum Exploration & Development, PetroChina, Beijing 100083, China; liangc69@petrochina.com.cn (C.L.); kongxwen@petrochina.com.cn (X.K.); wp2011@petrochina.com.cn (P.W.)
[2]   Petroleum Engineering School, Southwest Petroleum University, Chengdu 610500, China
[3]   CNPC Engineering Technology R&D Company Limited, Beijing 100083, China; wanghaigedri@cnpc.com.cn
[*]   Correspondence: konglulin1986@163.com or konglulin@petrochina.com.cn (L.K.); swpu_wzw@163.com (Z.W.)

Abstract: Well structures with ultra-long sections have become one of the most applied technologies in the field of shale gas development. While there have been many technical challenges, enhancing the breaking efficiency and stability of polycrystalline diamond compact (PDC) bits has become an essential issue of focus. Since 2013, the well structure in the Duvernay area has been optimized multiple times, and the rate of penetration (*ROP*) of the entire wellbore has nearly doubled. However, there are significant differences in terms of the performances of different PDC bits, and there is still room for improvement to optimize these drill bits. For this reason, a confined compressive strength test was conducted to obtain the rock mechanical parameters from shale cores extracted from the long horizontal section. Using these data, a finite element model (FEM) was developed with a corresponding scale. A calibration of the elastic-plastic damage constitutive models was then performed using the FEM. The breaking mechanism of three different PDC bits was examined using a "PDC bit-bottom hole" interaction FEM model, facilitating guidance for bit selection and design optimization: (1) The type B PDC bit, which has four blades and 20 cutters, exhibited the highest mechanical specific energy (*MSE*) and the lowest vibration across three directional mechanical characteristics. This design is recommended for engineering applications. (2) Lower axial vibrations were produced when the CDE was used as the rear element when compared to those when using the BHE. However, an increase within an acceptable range was observed in the *TOB* and circumferential vibrations. Thus, for redesigning work on the type B bit, the assembly of the CDE is suggested. (3) A decrease in the *MSE* and vibration in three directional mechanical characteristics was observed when the depth of cut (*DOC*) was varied between 1.5 and 2.0 mm. A broadening in the range of lateral forces was noted when a *DOC* of 2.0 mm was used. Therefore, for the redesign of the type B bit, the assembly of CDEs as rear elements at a *DOC* of 1.5 mm is recommended. In conclusion, a new practical method for the selection and optimization of PDC bit design, based on rock mechanics and the FEM theory, is proposed.

Keywords: shale gas; long horizontal section; FEM modeling; bit selection; optimization design of PDC bits; Duvernay area

1. Introduction

The main countries and regions that exploit shale gas almost all use an ultra-long horizontal well structure to enhance production and reduce development costs significantly. This well structure has become one of the most applied technologies in the field of shale gas development, and enhancing the breaking efficiency and stability of PDC bits is necessary for providing technical support. Hence, theoretical and applicational studies have been

conducted, for example, in the Duvernay area in Canada. Since 2013, enhancements have been made three times on the ultra-long horizontal section, where the measured depth exceeds 7000 m, and the rate of penetration (*ROP*) has improved by approximately one time, with minimal wear observed on the retrieved bits. However, even recently, two to four trips are still required to complete the drilling engineering of the horizontal section. The performance of each type of PDC bit is influenced by intricate engineering parameters and the frictional resistance along the well trajectory. Therefore, the breaking efficiency and stability of certain bit types are not easily assessed via engineering phenomena. As depicted in Table 1, the footage and *ROP* for each type of PDC bit fluctuate. To minimize the number of trips and associated costs, further studies on bit selection and design improvements that employ a controllable method and context are imperative. Each type of PDC bit incorporates a series of fundamental structures, including cutting and hydraulic structures. This study focuses on the cutting structure. This structure comprises a specific number of blades, with each blade housing a set number of cutting elements based on its radial profile. The cutting elements are categorized into main and rear elements based on their relative position on each blade. The rock-breaking efficiency is predominantly determined by the number and shape of these main elements, whereas the rear element primarily aids the breaking process. The mechanism by which the rear element provides assistance varies, dependent on its geometric shape and position relative to the main element.

Table 1. Historical usage of PDC bits in Duvernay area, Canada.

Year	Well	Type of Bit	Main Features				Footage (m)	*ROP* (m/h)
			Number of Blades	Number of Main Elements	Main Elements	Rear Elements		
2020	E	A	5	24	V-shape cutters	BHEs	380	18.77
		B	4	20	Planar cutters	(Ball head element)	3396	47.66
2021	F	A	5	24	V-shape cutters	BHEs	487	27.83
		B	4	20	Planar cutters		628	44.07
		B	4	20	Planar cutters		2088	50.31
		B	4	20	Planar cutters		944	48.41
2022	G	C	5	18	Planar cutters	None	2995	44.53
	H	C	5	18	Planar cutters	None	2535	45.20

The selection and improvement of designs for bits rely on engineering performance and are affected by uncertainty in engineering parameters. There is typically a compromise between the breaking efficiency and stability, which does not reflect the improved performance due to specific design features. Based on this situation, an experiment, a simulation, and engineering studies on various design features were conducted. The stress areas of nine types of profiles of PDC bits were modeled according to the International Association of Drilling Contractors (IADC) [1]. The results indicate that the shallower inner cone forms a larger area of high stress, while the outer cone has a smaller impact on the propagation of stress at the bottom of the wellbore.

The tangential mechanical response and breaking work based on the radial location of the bit profile were analyzed. The results indicate that the nasal area demonstrates the highest breaking work, while the internal cone angle profoundly influences the stress level across the entire radial profile [2]. Finite element modeling (FEM) offers a simpler and more feasible approach when compared to experimental methods, and semi-quantitative simulations can adequately represent the effects of various cutting structure features, even in the absence of experimental support [3]. The *ROP* and torque on bit (TOB) were studied for different drilling parameters using a PDC bit, leading to the development of recommended usage guidelines for the designed drill bit [4]. A PDC bit featuring annular grooves on its blades was designed and tested to determine its breaking efficiency, as well as axial and circumferential mechanical characteristics based on experimental

data [5]. In summary, the impacts of diverse design features on the breaking process were discerned via a semi-quantitative analysis using the FEM method. Experimental methods are considerably more costly, often depending on intricate manufacturing techniques, the prototyping of various PDC bits, and engineering trials with an extremely low margin for error and complicated manual interference [6–8]. However, most of the highlighted simulation studies have centered primarily on effects related to the profile, single cutter, and drilling parameters of a singular type of bit, with only a handful exploring bit selection and further design considerations.

Three-dimensional (3D) models of three types of PDC bits, as listed in Table 1, each having distinct features on their cutting structures, are recreated in accordance with PDC bit design theories. Based on prior studies [9–13], the rock mechanical parameters obtained from triaxial compressive tests were utilized to calibrate the constitutive models, ensuring the scale modeling aligned with the experiments. The mechanical specific energy and stability in three directions for each of the three PDC bit types were then examined. Further improvements were pursued based on the results of the bit selection. This study provided a theoretical backing and pioneering insights for bit selection and design enhancements.

2. Methodology

2.1. Calibration of Constitutive Models

To calculate cohesion C and friction angle Φ using the Mohr–Coulomb method, two compression tests under different confinement pressures were required. Given that the vertical depth of the long horizontal section was approximately 3000 m and density of the drilling fluid ranged from 1.0 to 1.01 g/cm^3, the confining pressures in the experiment aimed to replicate the pressure conditions at the bottom of the hole. Consequently, using the equation $P = \rho g h$ (where P represents the bottom hole pressure in Pa, ρ represents the drilling fluid density in g/cm^3, and h indicates the vertical depth of the bottom hole in m), a confinement of 30 MPa was established. Another confining pressure was set at 15 MPa to calculate cohesion C and friction angle Φ and to facilitate further studies on PDC bits in sections with a vertical depth of 1500 m. Samples with a height of 50 mm and diameter of 25 mm were extracted from downhole cores.

Triaxial compressive tests were conducted under confining pressures of 15 MPa and 30 MPa (see Figure 1). As illustrated in Figure 1b, the red curves indicate radial stress–strain relation, and blue curves indicate lateral stress–stain relation. From the stress–strain curves of the tests, it was observed that shale sample sequentially underwent a near linear elastic stage, plastic stage, and strength degradation stage after triaxial compressive strength (*TCS*).
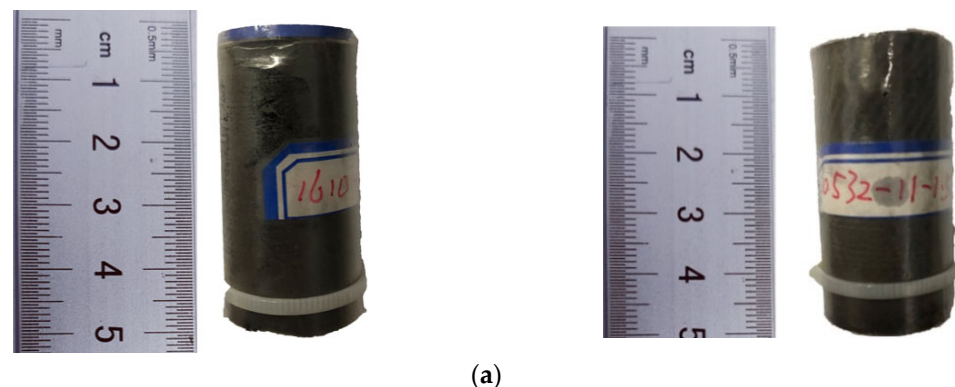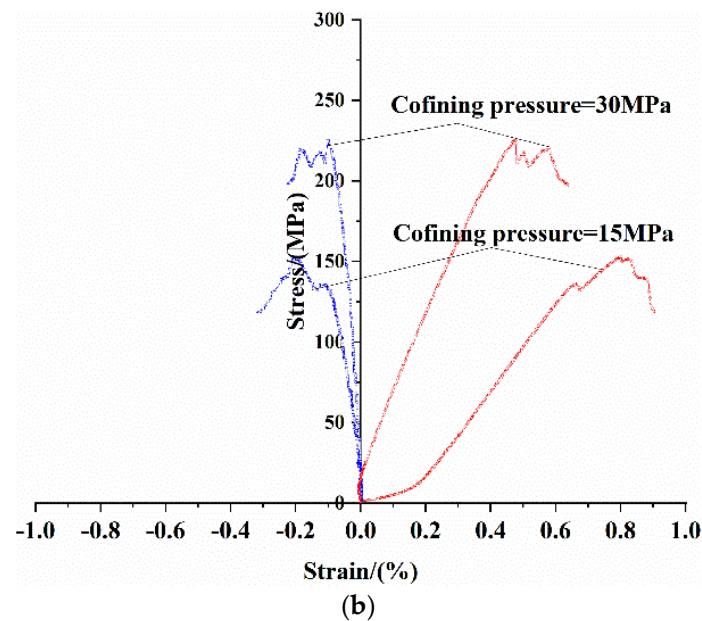

(**a**)

Figure 1. *Cont.*

Figure 1. Triaxial mechanical experiment conducted on shale samples. (**a**) Samples after the experiment (confining pressure is set to 15 MPa and 30 MPa); (**b**) stress–strain curves.

The derived rock mechanical parameters are listed in Table 2.

Table 2. Rock mechanical parameters of shale.

Confining Pressure/MPa	ρ/g/cm^3	E/GPa	TCS/MPa	μ/Decimal	Φ/°	C/MPa
15	2.41	28.08	152.90	0.23	40.96	18.43
30	2.73	50.16	225.00	0.17		

Where E denotes Young's modulus, GPa; ρ denotes density of rock sample, g/cm^3; TCS denotes triaxial compression strength, MPa; μ—i denotes Poisson's ratio, decimal; Φ denotes friction angle, °; and C denotes cohesion, MPa.

Based on observed experimental phenomena, a linear elastic model was employed to characterize the mechanical response of shale under load. A suitable strength criterion is essential for accurately modeling the mechanical response during non-linear yielding and hardening stages. Common strength criteria encompass the Mohr–Coulomb criterion, Drucker–Prager criterion, Griffith criterion, and Murrel's generalization of Griffith's criterion. In studies focusing on the rock breaking process, cracks were overlooked due to the influence of drilling mud, displaying dilation characteristics under shear damage. Therefore, the Drucker–Prager criterion, which considers intermediate principal stress, has been widely adopted in modeling the mechanical response of the bit–shale interaction process [10–13].

Yield surface function of Drucker–Prager criterion is provided in Equations (1) and (2) [10].

$$F = t - p \tan \beta - d \tag{1}$$

$$t = \frac{q}{2} \left[1 + \frac{1}{k} - \left(1 - \frac{1}{k} \right) \left(\frac{r}{q} \right)^3 \right] \tag{2}$$

where p denotes equivalent compressive stress, MPa; d denotes cohesion of shale sample, MPa; β denotes intercept on yield surface of p–t space, MPa; t denotes partial stress due to the influence of principal stress on yield surface, MPa; and K denotes plastic flow stress ratio, decimal, $0.778 \leq K \leq 1$. Furthermore, in the study, classical Drucker–Prager criterion

was adopted and $k = 1.0$; q denotes deviatoric stress, MPa; and r denotes third deviator stress component, MPa.

The classic Drucker–Prager criteria expressed in Equations (1) and (2) are shown in Figure 2.
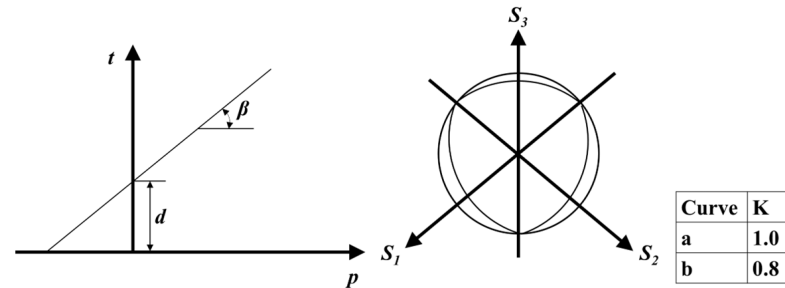

Curve	K
a	1.0
b	0.8

Figure 2. Yield surfaces of Drucker–Prager in the *p-t* plane and π plane.

Furthermore, true stress σ_{true} and equivalent plastic strain $\varepsilon_{ln}{}^{pl}$ derived from stress–strain curve are necessary to describe the mechanical response in hardening and damage stage (see Equations (3) and (4)). Specially, the relation between damage index D and equivalent plastic strain $\varepsilon_{ln}{}^{pl}$ was adopted to describe the mechanical response in progressive damage stage. As shown in Figure 3, it is assumed that damage stage begins when the stress response of shale reaches strength stress with $D = 0$ and $\varepsilon_{ln}{}^{pl} = \varepsilon_0{}^{pl}$. As the material softens, D gradually increases from 0 to 1, and the stiffness of material is 0 when $D = 1$ (and $\varepsilon_{ln}{}^{pl} = \varepsilon_f{}^{pl}$ at the same time). Meanwhile, corresponding finite element mesh is considered to be a failure and removed.
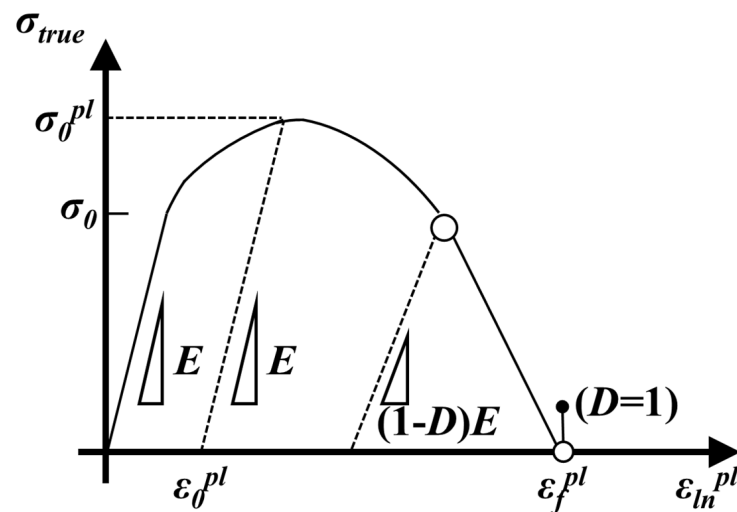

Figure 3. Illustration of the progressive damage stage of rock.

In FEM theory concerning gradual damage in expansive formation models, the stress–strain relationship no longer depicts the mechanical response of shale once damage has occurred. Utilizing this relationship introduces a pronounced mesh dependency due to strain localization, commonly referred to as the size effect. Consequently, an alternative approach is required to trace the strain-softening branch of the stress–strain response curve. To circumvent the size effect due to the finite element size, the strain–stress relationship should be transposed to an equivalent stress–displacement relationship. This approach allows the gradual damage stage to be represented by a stress–displacement response as opposed to a stress–strain response. In this study, the equivalent failure displacement was selected as the direct failure parameter for shale, determined using Equations (5)–(8). It is worth noting that the application of the stress–displacement concept in the FEM model mandates a characteristic length, L, tied to an integration point. During its specific

implementation, the shale's geometry should be meshed uniformly across various modeling scenarios. The value for *L* should then be derived from Equation (5).

$$\sigma_{true} = \sigma_{nom}(1 + \varepsilon_{nom}) \tag{3}$$

$$\varepsilon_{\ln^{pl}} = \ln(1 + \varepsilon_{nom}) - \frac{\sigma_{true}}{E} \tag{4}$$

$$L = \sqrt[3]{V_{element}} \tag{5}$$

$$\begin{cases} u_f^{pl} = L\varepsilon_f^{pl} \\ u^{pl} = L\varepsilon^{pl} \end{cases} \tag{6}$$

$$D = \frac{L\varepsilon^{pl}}{u_f^{pl}} \tag{7}$$

$$\begin{cases} \varepsilon_{\ln^{pl}} \le \varepsilon_f^{pl} \\ u_{\ln^{pl}} \le u_f^{pl} \end{cases} \tag{8}$$

where σ_{true} denotes true stress, MPa; σ_{nom} denotes nominal stress, MPa; ε_{nom} denotes nominal strain, decimal; $\varepsilon_{\ln^{pl}}$—denotes equivalent plastic strain, decimal; *E* denotes Young's modulus, GPa; *D* denotes damage index, decimal, $0 \le D \le 1$; ε_f^{pl} denotes the equivalent plastic strain when stiffness of material is 0, decimal; $\varepsilon_{\ln}^{pl}$ denotes equivalent plastic strain, decimal; $u_{\ln}^{pl}$ denotes equivalent plastic displacement of material, mm; u_f^{pl} denotes equivalent plastic displacement when *D* = 1, mm; *L* denotes feature length of finite element mesh, mm; and $V_{element}$ denotes volume of finite element mesh, mm^3.

A uniform-scale FEM model was constructed based on the previously mentioned theory and parameters. This model had a confining pressure of 30 MPa, reflecting the bottom hole pressure for the long horizontal section in the study area, and its shale geometry matched that of the experiment. The model was analyzed using an explicit dynamic procedure. Observations from this analysis showed that the fracturing mode is characterized by shear damage (See Figure 4).
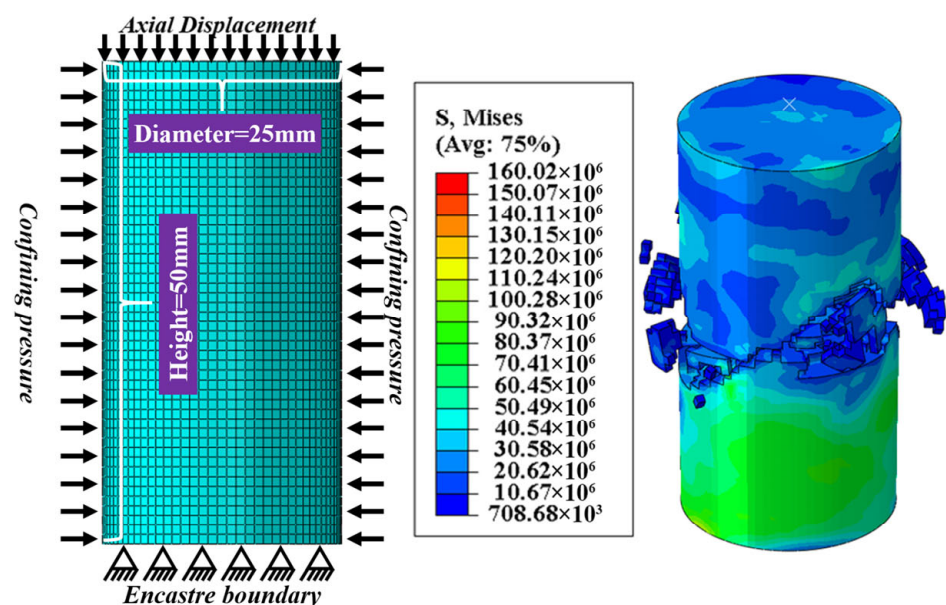

Figure 4. FEM model aligned with the scale of the compressive test, accompanied by a contour plot of the modeling results.

The red curve depicts the experimental results, whereas the blue curve illustrates the simulation outcomes, as shown in Figure 5. The stress–strain curve derived from the simulation closely mirrors the mechanical response observed in laboratory experiments across the elastic, plastic, and damage phases. Consequently, the constitutive models and rock mechanics parameters utilized are deemed appropriate for subsequent simulation studies focusing on the PDC bit–shale interaction process.
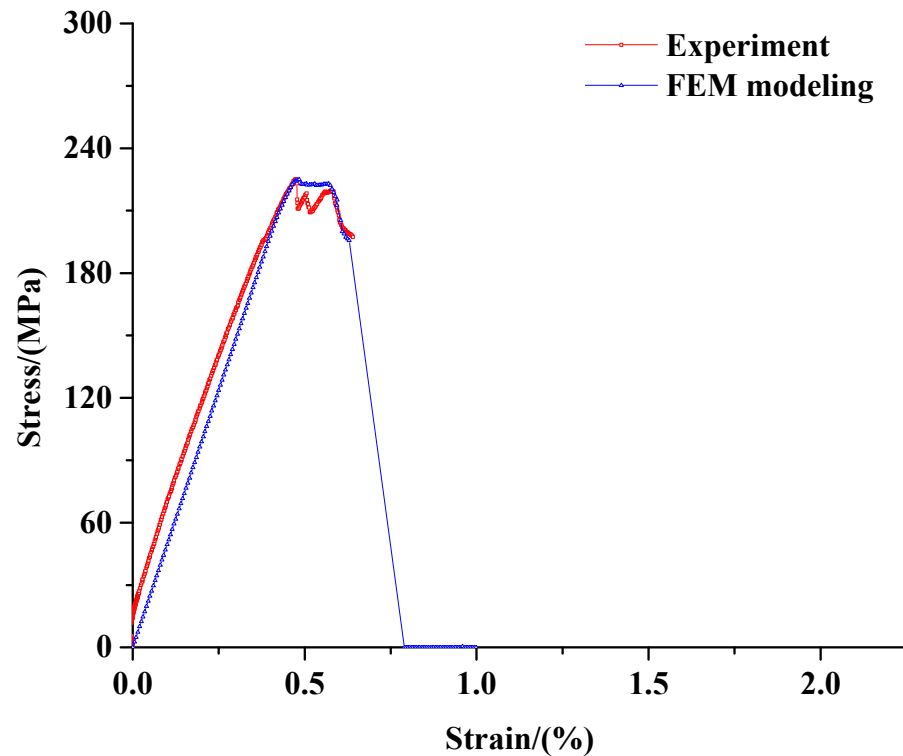
Figure 5. Stress–strain curve of shale (when confining pressure was 30 MPa).

2.2. D Model Reconstruction of PDC Bit and FEM Model of Rock Breaking Process

At the onset of the 3D model reconstruction, determining the radial profile and corresponding arrangement of both main and rear elements was crucial. By employing image analysis on PDC bit visuals, the 3D distribution in a circumferential view underwent iterative adjustments. Ultimately, the reconstructed 3D model accurately represented the cutting structure of the actual engineering PDC bit.

Critical parameters of the cutting structure, which profoundly influence the PDC bit's breaking process, were measured using image analysis. These parameters encompassed the distribution and geometric width of blades, slot depth, and the diameter and number of primary cutting elements. Owing to the absence of a precise side view, crown profile parameters were kept consistent, barring a few gauge sections. Initially, the inner cone angle was designated as 75°. Based on design experience, the rack angles were assigned values of 12°, 16°, 18°, and 35° for the inner cone, nose, shoulder, and gauge, respectively. Using the observed parameters, radial and circumferential cutter arrangements are conducted, leading to the completion of the entire 3D model, as shown in Figure 6. Red curves represent radial profiles and the arrangement of rear elements; black curves denote the radial blade profiles and arrangements of gauges; and blue, pink, and green curves illustrate the radial profiles and positioning of main elements in the inner cone, nose, and shoulder, respectively. It is vital to highlight that the PDC bit's hydraulic system (including flow channels, slots, and nozzles) is presented purely for visual purposes as the study emphasizes cutting structures.
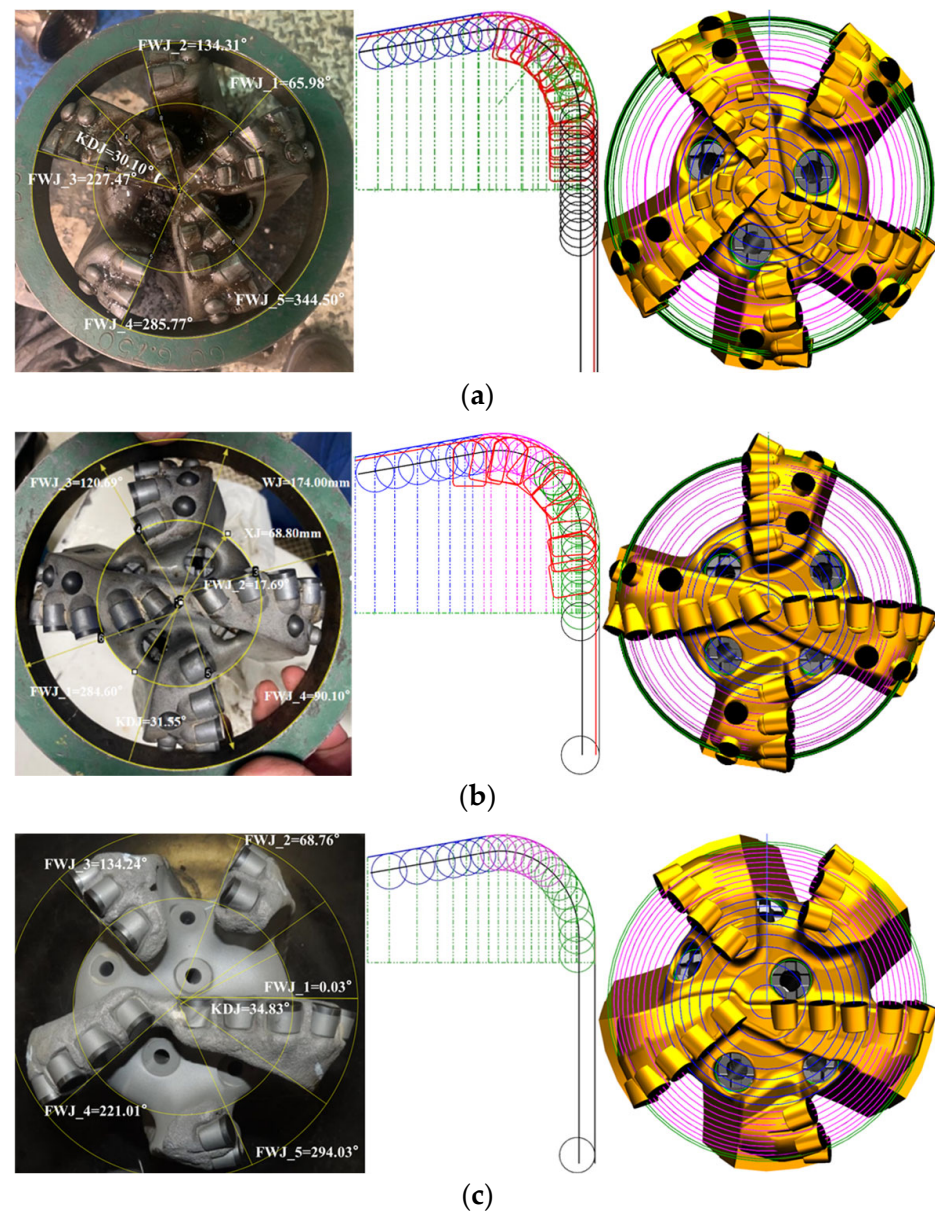
Figure 6. Image analysis and 3D reconstruction of three types of PDC bits. (**a**) Type A PDC bit (5 blades, V-shape cutter as main cutting element). (**b**) Type B PDC bit (4 blades, planar cutter as main cutting element). (**c**) Type C PDC bit (5 blades, planar cutter as main cutting element).

Based on calibrated constitutive models and reconstruction of three types of PDC bits, an FEM model for the interaction between the PDC bit and shale was formulated and resolved via an explicit dynamic procedure, as depicted in Figure 7. This allowed for the differences in breaking efficiency and stability to be discerned without the intricacies of an engineering situation. The rock mechanical parameters used are in line with the results under confining pressure of 30 MPa as listed in Table 2. To uncover the mechanical attributes of the breaking process, the loading mode was set to speed control. The dynamic boundary close to the bit mirrored the parameters gauged by measurement while drilling (MWD) technology with a rotational speed of 288 r/min and an *ROP* of 63.3 m/h. Mechanical characteristics in three directions, illustrated in Figure 8, are derived once the FEM models are processed using the dynamic explicit algorithm. These characteristics include the required weight on bit (WOB), *TOB*, and lateral force.
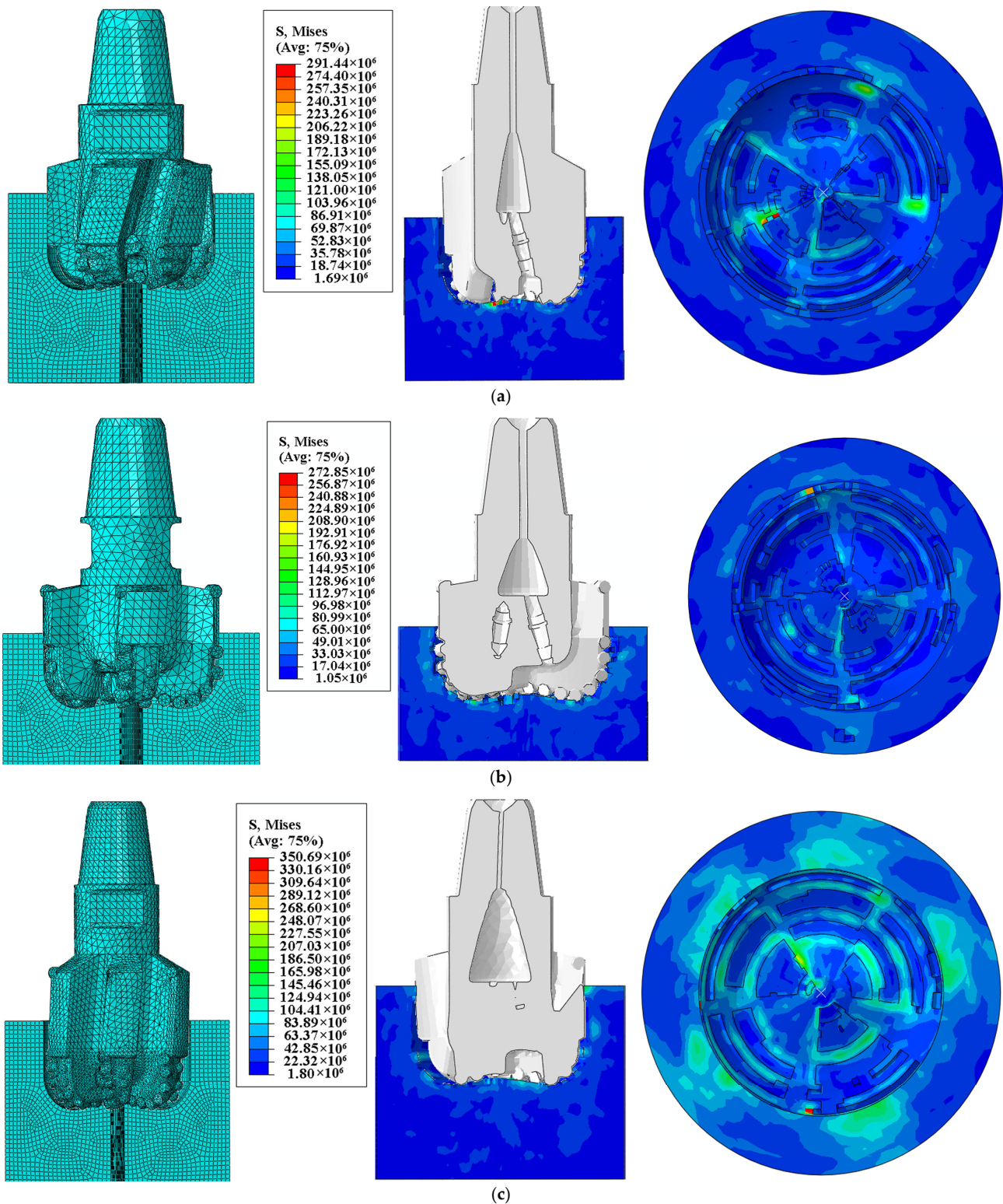
Figure 7. FEM model and contour plot of PDC bit–shale interaction process. (**a**) PDC bit–shale interaction when Type A is adopted. (**b**) PDC bit–shale interaction when Type B is adopted. (**c**) PDC bit-shale interaction when Type B adopted.
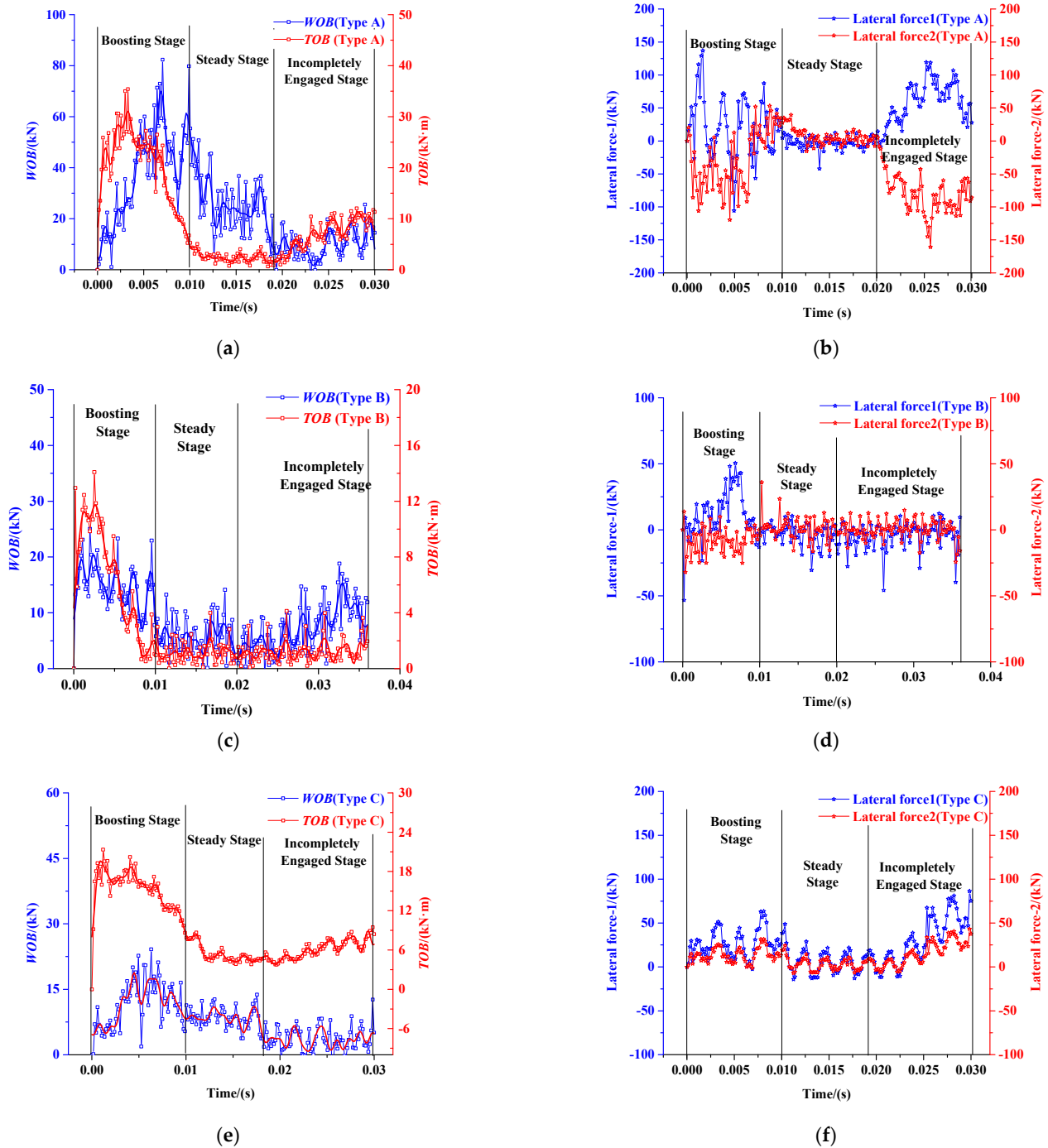
Figure 8. Time history curves of three-directional mechanical characteristics. (**a**) *WOB* and *TOB* of type A. (**b**) Lateral force of type A. (**c**) *WOB* and *TOB* of type B. (**d**) Lateral force of type B. (**e**) *WOB* and *TOB* of type C. (**f**) Lateral force of type C.

The PDC bit progressively engages with the bottom hole due to the combined effects of impact and rotation, initiating the shale breaking process, as illustrated in Figure 8. The time history curve of WOB, TOB, and lateral force has three distinct stages: a boosting stage, a steady stage, and an incompletely engaged stage, with the curves of Type A serving as a reference. From t = 0–0.01 s, values oscillate, increasing and then decreasing. During this interval, the bit gradually engages with the bottom hole. The energy accumulated during this phase is released to overcome the static friction process. Between t = 0.01 and 0.02 s, the values stabilize. The static friction transitions to dynamic friction, and the mechanical

response achieves a relatively dynamic equilibrium. For time t > 0.02 s, some of the cutters begin to interact with the next layer of elements, encountering fewer elements than other parts of the cutting structure. This signifies that the engagement between the bit and bottom hole is not wholly consistent, marking this phase as the incompletely engaged stage. Given these observations, statistical calculations and analyses are centered primarily on the values of the three directional mechanical characteristics observed during the steady stage.

3. FEM Modeling Results

3.1. Bit Selection Based on Statistical Results of FEM Analysis

MSE, representing the mechanical work needed to break a unit volume of rock, was initially introduced in 1965 [14]. Subsequent models tailored to specific engineering conditions have been developed based on this original concept [15–18]. This study focuses on the stage of dynamic friction, excluding factors such as the drilling fluid, wear damage, and mechanical efficiency. Hence, the model by Pessier, which considers the dynamic friction coefficient, was selected (see Equation (9)).

$$MSE = WOB\left(\frac{1}{D_b} + \frac{13.33\mu_b RPM}{A_b ROP}\right)$$
$$\mu_b = 36\left(\frac{T}{D_b WOB}\right)$$

$$(9)$$

where *MSE* denotes the mechanical specific energy, 10^3 MPa; *WOB* denotes the weight on bit in kN; *RPM* denotes the rotational speed per minute in r/min; *T* denotes the torque on bit in kN·m; A_b denotes the area of the PDC bit in mm^2; D_b denotes the diameter of the PDC bit in mm; *ROP* denotes the rate of penetration in m/h; and μ_b denotes the dynamic friction coefficient as a decimal.

The *MSE* model by Pessier was employed to assess the breaking efficiency, using the aforementioned statistical results. The calculated outcomes are illustrated in Figure 9. The standard deviations of the *WOB* and *TOB* were determined to describe the axial and circumferential vibration amplitude. The deviation value is represented on the Y-axis, analogous to the corresponding variable. Under consistent ROP–RPM dynamic boundaries, the average *WOB* required, *TOB* withstood, and *MSE* for type B were 5.91 kN, 1.16 kN·m, and 34.64 MPa (see Figure 9a), respectively. The range of lateral force was between −5.94 and 10.48 kN (see Figure 9b), which is the lowest among the three types. Comparing efficiency and stability, type A and type B exhibit minimal differences in stability, with both significantly outperforming type C. However, the *MSE* for types A and C showed an improvement of 297.73% and 44.60%, respectively, over type B. This suggests that, for drilling in long horizontal sections, type B with its four blades is the optimal choice. The V-shape cutters were not deemed appropriate for this particular long horizontal section in the area under study. Therefore, a PDC bit featuring a planar cutter as the primary cutting element, complemented by rear elements, is essential to minimize vibration.

3.2. Improving Design Based on Results of Bit Selection

In Section 3.2, we discussed the bit selection, in which an appropriate cutting structure for the aforementioned shale gas area was identified. To augment the efficiency and stability of type B, this cutting structure underwent further optimization. The key adjustable features of the cutting structure encompass the crown profile [1], the rack/side angle of the cutting element [19], the spacing between adjacent cutters [20], the design of cutters placed on the front or rear [21], and the blade structures [22], among others. In this study, our focus was on refining the shape of the cutters positioned at the rear of the blades. Research by Azar, Michael, Gunawan, and Fatah highlights that the conical diamond element (CDE) can induce a pre-cracking effect on the bottom hole based on engineering tests [23,24]. This results in the creation of an unconfined groove and stress area for primary cutting elements (see Figure 10). Concurrently, it can diminish the vibration of the PDC bit. This suggests that employing a CDE can enhance the *MSE* and curtail vibrations.
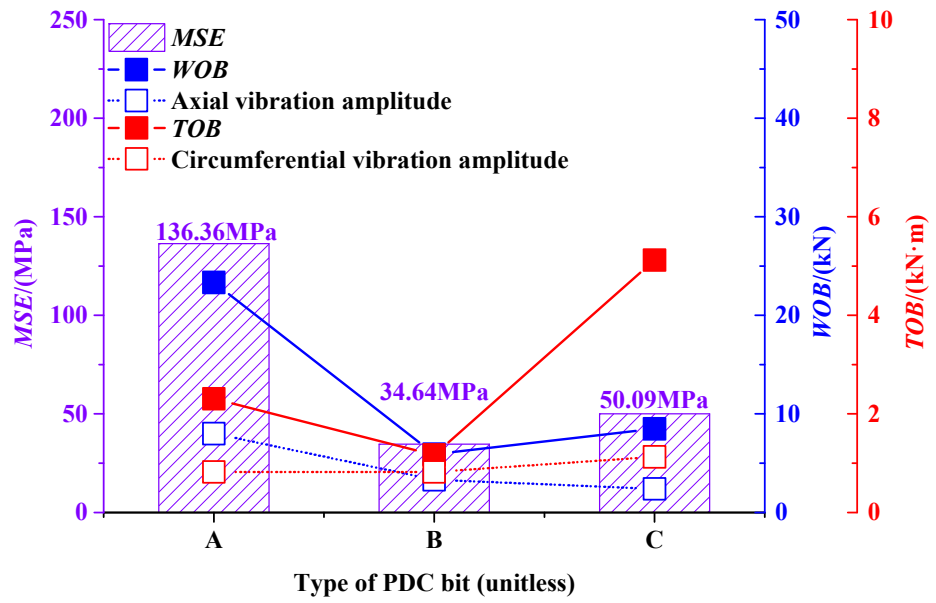
(a)
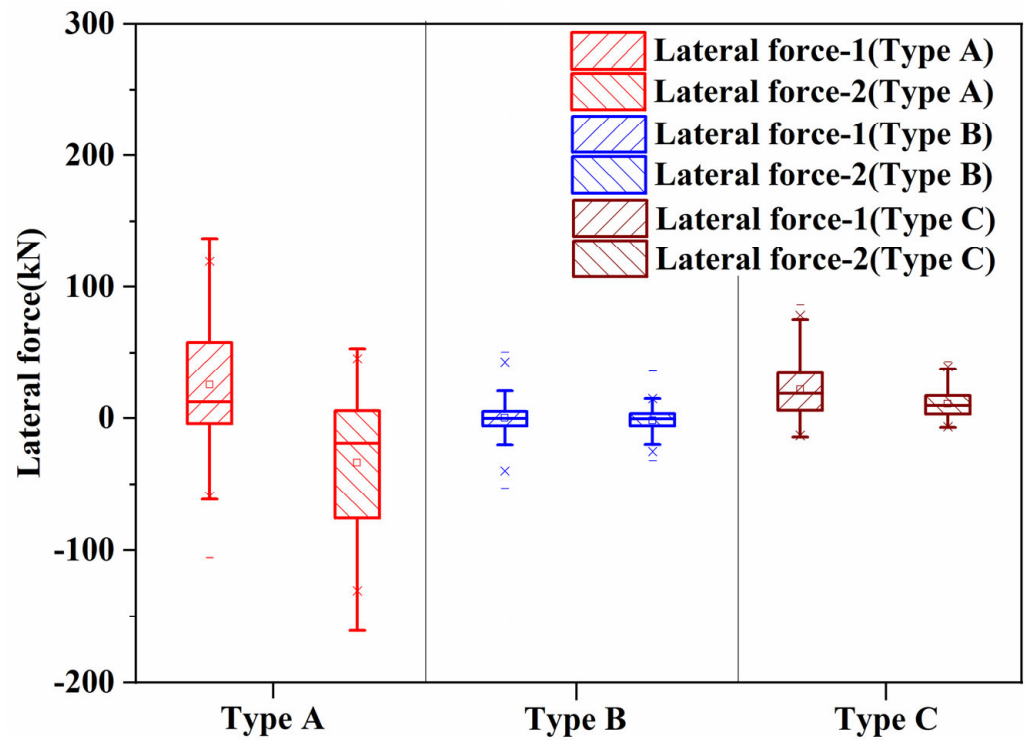
(b)

Figure 9. Comparison of *MSE* when different types of PDC bits were used. (**a**) Comparison of *MSE*, *WOB*, and *TOB*. (**b**) Comparison of lateral forces.
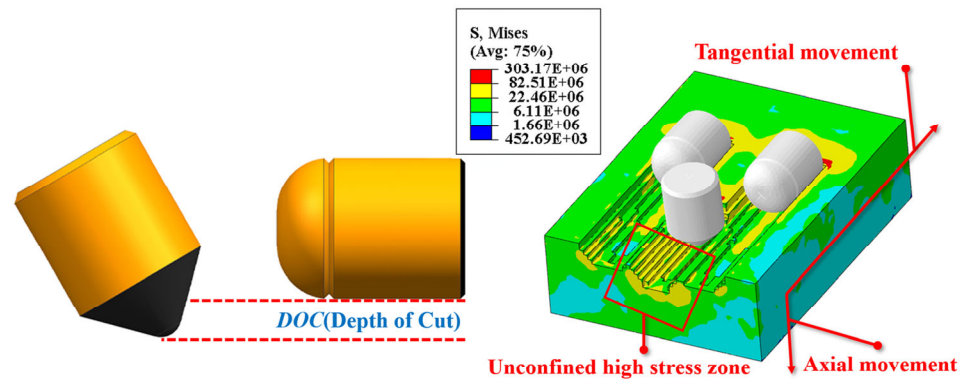
Figure 10. Illustration of pre-cracking effect by CDE assembled with certain *DOC*.

To understand the impact of the rear elements' shape and the *DOC* between the front and rear elements, we embarked on a study to optimize the cutting structure. The details of this optimization are presented in Table 3. This was executed based on the redesigned 3D models of the PDC bit (see Figure 11) and the established FEM models.

Table 3. Simulation scheme of different cutting elements and different *DOC*s.

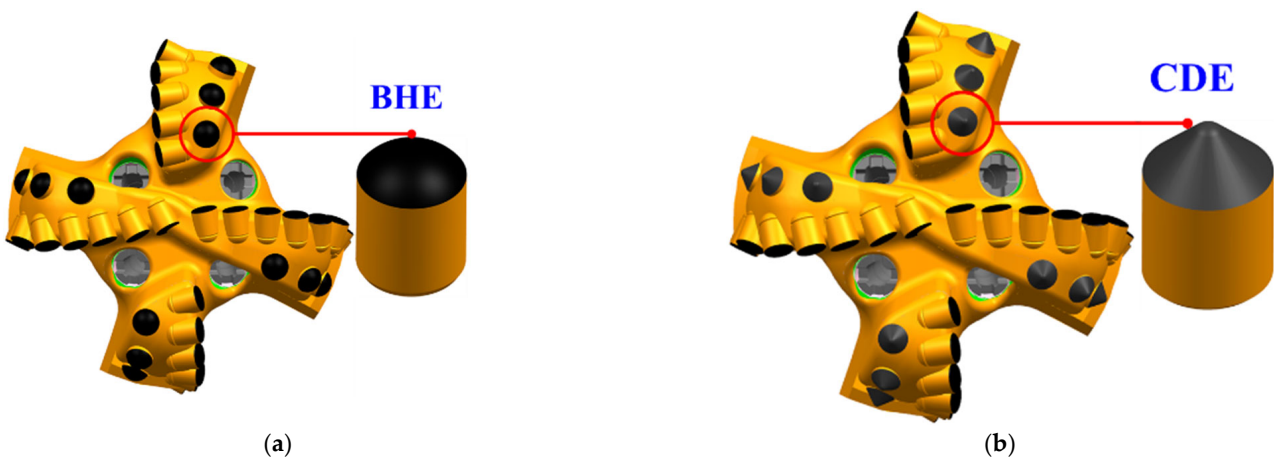| Rear Elements		BHEs		CDEs	
DOC, mm	0.5	1.0	1.5	2.0	2.5
Kinematic boundaries	Rotational speed = 288 r/min, *ROP* = 63.3 m/h				

(**a**)

(**b**)

Figure 11. Bit assembled with planar cutters as main elements and BHEs or CDEs as the rear elements. (**a**) Type B with BHEs assembled. (**b**) Type B with CDEs assembled.

The FEM models, which considered bits with varying *DOC* values and distinct rear element shapes, were analyzed. The average and standard deviation values of the *WOB* and *TOB*, along with the *MSE*, are presented in Figure 12, while the ranges of the lateral forces can be viewed in Figure 13. For the original history curves of the *WOB*, *TOB*, and lateral forces, please refer to Appendix A.
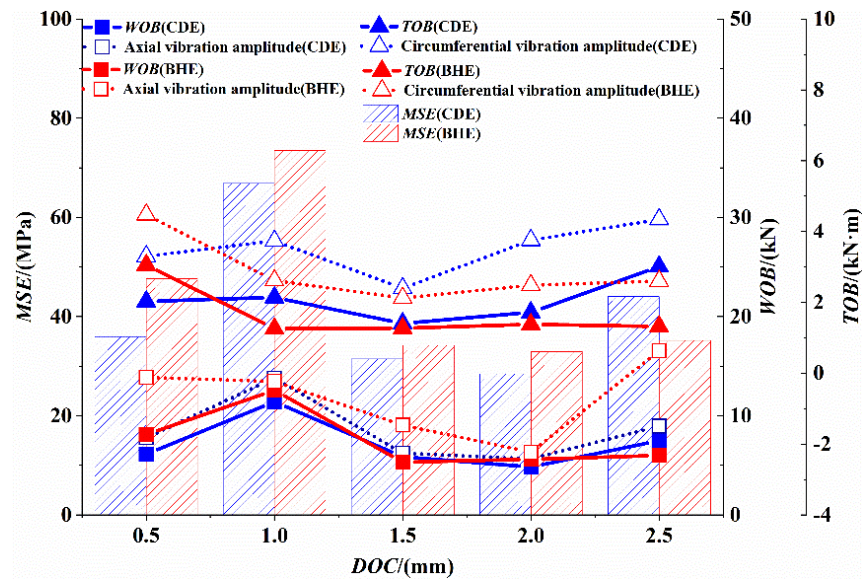
Figure 12. Comparison of *MSE*, *WOB*, and *TOB* at different values of *DOC*.
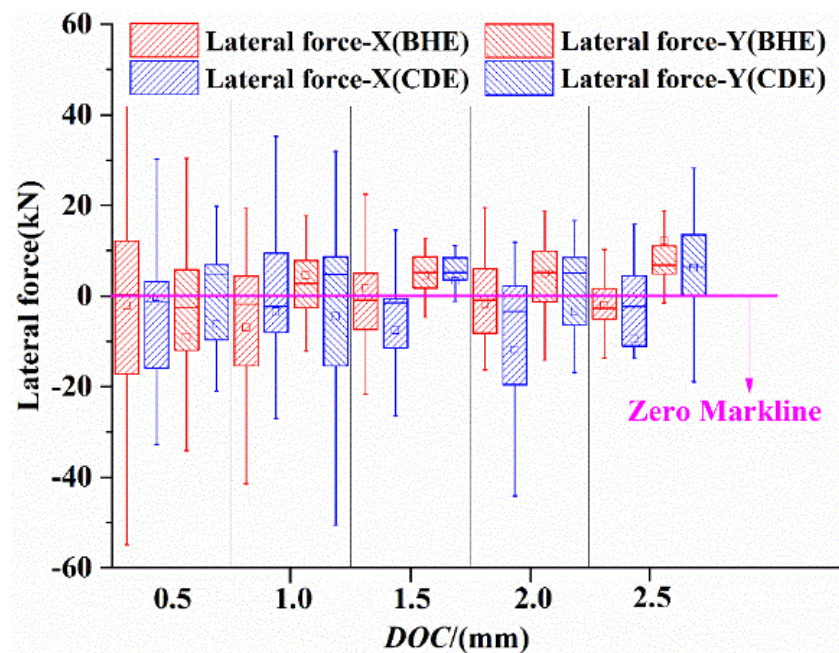

Figure 13. Comparison of lateral forces at different values of *DOC*.

In Figure 12, as the *DOC* rises incrementally from 0.5 mm to 2.5 mm, there is a noticeable trend in the *MSE* and *WOB*: they initially increase, then decrease, and finally surge again. This suggests that greater *DOC*s boost the cutting depth of the primary cutting element, thereby enhancing the efficiency of each main element. However, if the *DOC* is excessively high, then the energy expended in rock breaking is partly wasted on vibrations due to the diminished damping effects of the rear element. Particularly noteworthy are the findings at *DOC* = 1.5 mm and *DOC* = 2.0 mm, where the energy consumption is noticeably lower in both rear assembly conditions, irrespective of the element type. Moreover, the use of CDEs results in reduced MSE values. Our observations also revealed that the bits with CDEs exhibited diminished axial vibration amplitude when compared to those assembled with BHEs. Conversely, they displayed an increased circumferential vibration, suggesting that CDEs facilitate bit insertion into the bottom hole while minimizing axial bouncing. However, in most of the *DOC* conditions for which the *DOC* is more than 0.5 mm, the

TOB and circumferential amplitude were comparable or even higher than when BHEs were used. This implies that, with CDEs in place, there is a larger volume of rock that needs breaking in the circumferential direction due to improved insertion conditions. It is worth noting that, while energy requirements are substantially lower at *DOC* = 1.5 mm and *DOC* = 2.0 mm, the range of lateral forces is broader at *DOC* = 2.0 mm, as shown in Figure 13. Therefore, for the extensive horizontal sections in the study's shale region, it is recommended to incorporate CDEs as rear elements at a *DOC* of 1.5 mm during the redesigning of type B. This can potentially lead to fewer drilling trips with a significant reduction in energy consumption and acceptable vibration levels in all three directions, ensuring optimal bit performance.

4. Conclusions

In this study, for the first time, a novel practical method for the selection and optimization design of PDC bits based on rock mechanics and the FEM theory was introduced. Bit selection for three types of PDC bits was conducted using FEM modeling and adjusted rock mechanical constitutive models. The *DOC* between the main element and rear element was also investigated, leading to the following conclusions.

The shale samples from the long horizontal section in the Duvernay area exhibited a high brittleness (with a very short plastic stage) and a high *TCS* (152.86 MPa and 224.41 MPa at confining pressures of 15 MPa and 30 MPa, respectively). The elastic constitutive model, Drucker–Prager criterion, and asymptotic damage constitutive model accurately represented the mechanical response of the shale under load. These models are appropriate for analyzing PDC bit–shale interactions at a confining pressure of 30 MPa, which matches the bottom hole conditions of the study area's long section. The minimum *MSE* was noted when the PDC bit was assembled with four blades, suggesting that a planar cutter is preferable for drilling in the long horizontal section of the studied shale gas area. Rear elements that can reduce vibration levels are essential for inclination control. As the *DOC* increases, the cutting depth of the main cutting element and effective cutting area of each main element are enhanced, boosting the efficiency. However, if the *DOC* is too high, then some energy used for rock breaking is lost to vibration due to the overly diminished damping effect of the rear element, leading to a rise in *MSE*. With CDEs as the rear elements, the axial vibrations decreased compared to those when BHEs were used, but the *TOB* and circumferential vibrations slightly increased. For *DOC* values of 1.5 mm and 2.0 mm, even though the energy required for rock breaking was significantly reduced, a broader range of lateral forces was observed at *DOC* = 2.0 mm. Therefore, in redesigning type B, CDEs should be incorporated as rear elements at a *DOC* of 1.5 mm.

In summary, the type B PDC bit equipped with planar cutters as the primary element and CDEs as the rear elements at a *DOC* of 1.5 mm demonstrates a superior breaking efficiency and extended footage in drilling the long horizontal section of the Duvernay area.

The limitations of the method in the current study are as follows: (1) PDC bits were considered as rigid bodies and did not reflect the deformation of the PDC bits. Thus, future studies should examine the evaluation method for wear damage. Additionally, (2) the constitutive models adopted in this study only considered homogeneous material and did not describe the heterogenous characteristics of shale.

Author Contributions: L.K. and H.W. contributed to the study's conception and PDC bit design. Z.W. conducted the finite element modeling and analysis. M.C. wrote the manuscript. C.L., X.K. and P.W. conducted the experiments and wrote the first draft of the manuscript. All authors have read and agreed to the published version of the manuscript.

Conflicts of Interest: The authors declare no conflict of interest.
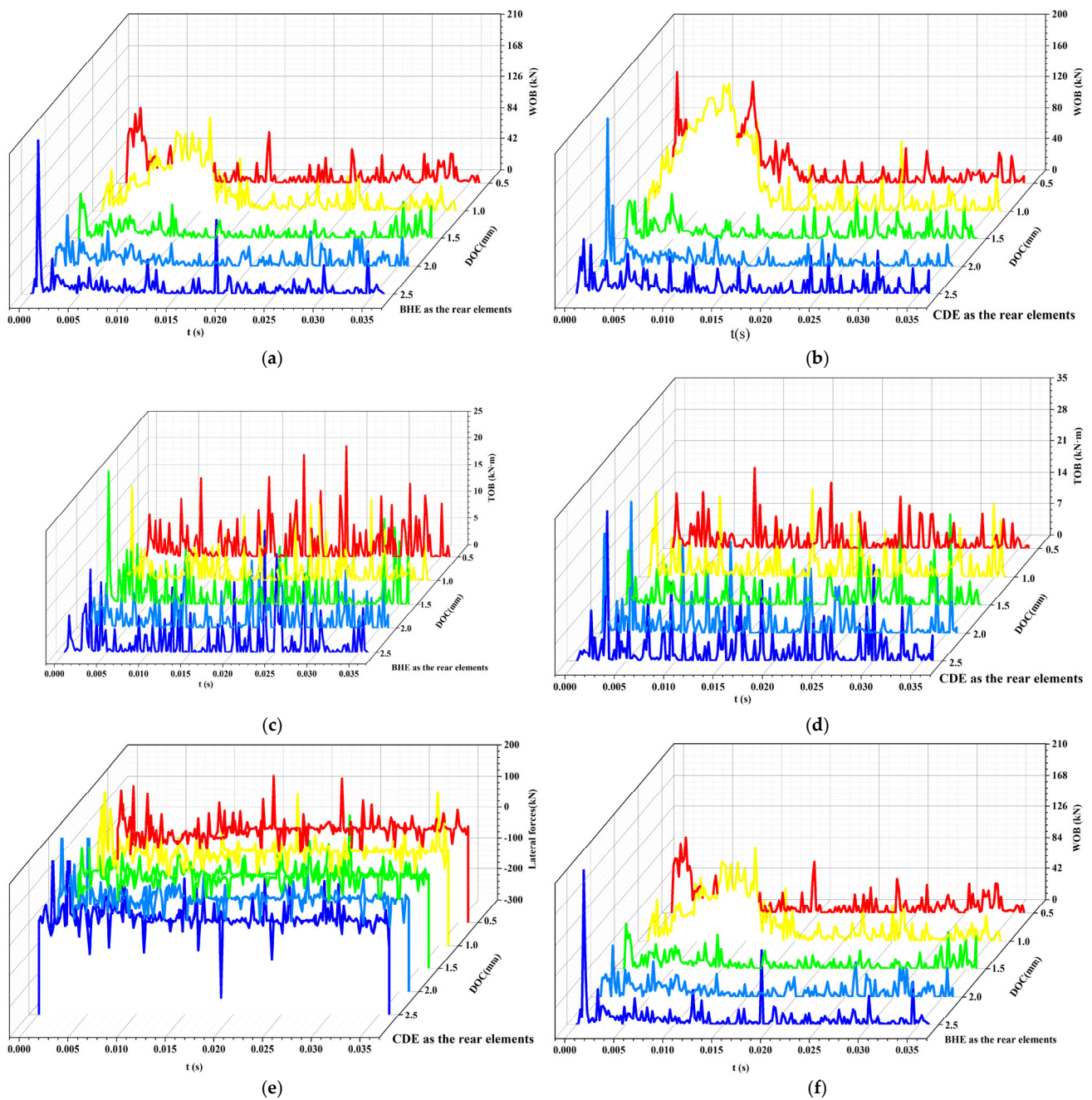
Appendix A

Figure A1. Three-directional mechanical characteristics. (**a**) Time history curve of *WOB* with BHE as rear elements. (**b**) Time history curve of *WOB* with CDE as rear elements. (**c**) Time history curve of *TOB* with BHE as rear elements. (**d**) Time history curve of *TOB* with CDE as rear elements. (**e**) Time history curve of lateral forces with BHE as rear elements. (**f**) Time history curve of lateral forces with CDE as rear elements.

References

1. Heydarshahy, S.A.; Karekal, S. Influences of bit profiles on possible fracture modes. *Pet. Explor. Dev.* **2017**, *44*, 667–674. [CrossRef]
2. Ju, P.; Wang, Z.Q.; Zhai, Y.H. Numerical simulation study on the optimization design of the crown shape of PDC drill bit. *J. Pet. Explor. Prod. Technol.* **2014**, *4*, 343–350. [CrossRef]
3. Pryhorovska, T.O.; Chaplinskiy, S.S.; Kudriavtsev, I.O. Finite element modelling of rock mass cutting by cutters for PDC drill bits. *Petrol. Explor. Dev.* **2015**, *42*, 888–892. [CrossRef]

4. Kuang, Y.C.; Zhang, M.M.; Feng, M. Simulation and Experimental Research of PDC Bit Cutting Rock. *J. Fail. Anal. Prev.* **2016**, *16*, 1101–1107. [CrossRef]
5. Huang, K.L.; Ai, Z.J.; Yang, Y.X. The improved rock breaking efficiency of an annular-groove PDC bit. *J. Petrol. Sci. Eng.* **2019**, *172*, 425–435. [CrossRef]
6. Yu, G.; Ning, K.; Tong, J.S. Optimization Selection of Bit and Application Research on PDC + Motor Combination Drilling Technique in the Desert Oilfield. *IOP Conf. Ser. Earth Environ. Sci.* **2019**, *310*, 022016. [CrossRef]
7. Hemphill, T.; Clarke, R.K. Effects of PDC-bit selection and mud chemistry on drilling rates in shale. *SPE Drill. Complet.* **1994**, *9*, 176–184. [CrossRef]
8. Rolf, P.; Michael, D.S.B.H. Hybrid Bits Offer Distinct Advantages in Selected Roller-Cone and PDC-Bit Applications. *SPE Drill. Complet.* **2011**, *26*, 96–103. [CrossRef]
9. Carrapatoso, C.; Da, F.; Sergio, A.B.; Inoue, N. New Developments for Single-Cutter Modeling of Evaporites Using Discrete Element Method. In Proceedings of the ISRM Conference on Rock Mechanics for Natural Resources and Infrastructure-SBMR, Goiania, Brazil, 9–13 September 2017.
10. Yang, Y.X.; Zhang, C.L.; Lin, M. Research on rock-breaking mechanism of cross-cutting PDC bit. *J. Petrol. Sci. Eng.* **2018**, *161*, 657–666. [CrossRef]
11. Liu, W.J.; Zhu, X.H.; Li, B. The rock breaking mechanism analysis of rotary percussive cutting by single PDC cutter. *Arab. J. Geosci.* **2018**, *11*, 192. [CrossRef]
12. Diarra, H.; Mazel, V.; Busignies, V. Sensitivity of elastic parameters during the numerical simulation of pharmaceutical die compaction process with Drucker-Prager/Cap model. *Powder Technol.* **2018**, *332*, 150–157. [CrossRef]
13. Schweiger, H.F. On the use of drucker-prager failure criteria for earth pressure problems. *Comput. Geotech.* **1994**, *16*, 223–246. [CrossRef]
14. Teale, R. The concept of specific energy in rock drilling. *Int. J. Rock Mech. Min. Sci. Geomech. Abstr.* **1965**, *2*, 57–73. [CrossRef]
15. Pessier, R.C.; Fear, M.J. Quantifying Common Drilling Problems with Mechanical Specific Energy and a Bit-Specific Coefficient of Sliding Friction. In Proceedings of the SPE Annual Technical Conference and Exhibition, Washington, DC, USA, 4–7 October 1992. [CrossRef]
16. Dupriest, F.E.; Koederitz, W.L. Maximizing Drill Rates with Real-Time Surveillance of Mechanical Specific Energy. In Proceedings of the SPE/IADC Drilling Conference, Amsterdam, The Netherlands, 23–25 February 2005. [CrossRef]
17. Hammoutene, C. FEA Modeled MSE/UCS Values Optimize PDC Design for Entire Hole Section. In Proceedings of the SPE North Africa Technical Conference and Exhibition, Cairo, Egypt, 20–22 February 2012. [CrossRef]
18. Amadi, K.; Iyalla, I. Application of Mechanical Specific Energy Techniques in Reducing Drilling Cost in Deep-water Development. In Proceedings of the SPE Deepwater Drilling and Completions Conference, Galveston, TX, USA, 20–21 June 2012. [CrossRef]
19. Chen, P.J.; Meng, M.; Ren, R. Modeling of PDC single cutter–Poroelastic effects in rock cutting process. *J. Petrol. Sci. Eng.* **2019**, *183*, 1063–1080. [CrossRef]
20. Chen, P.J.; Meng, M.; Miska, S. Study on integrated effect of PDC double cutters. *J. Petrol. Sci. Eng.* **2019**, *178*, 1128–1142. [CrossRef]
21. Akbari, B.; Miska, S.Z.; Yu, M. The Effects of Size, Chamfer Geometry, and Back Rake Angle on Frictional Response of PDC Cutters. In Proceedings of the ARMA 48th U.S. Rock Mechanics/Geomechanics Symposium, Minneapolis, MN, USA, 1–4 June 2014.
22. Zhang, Y.; Baker, R.; Burhan, Y. Innovative Rolling PDC Cutter Increases Drilling Efficiency Improving Bit Performance in Challenging Applications. In Proceedings of the SPE/IADC Drilling Conference, Amsterdam, The Netherlands, 5–7 March 2013. [CrossRef]
23. Azar, M.; White, A.; Segal, S. Pointing Towards Improved PDC Bit Performance: Innovative Conical Shaped Polycrystalline Diamond Element Achieves Higher ROP and Total Footage. In Proceedings of the SPE/IADC Drilling Conference, Amsterdam, The Netherlands, 5–7 March 2013. [CrossRef]
24. Gunawan, F.; Krisnanto, W.; Mardiana, M.R.; Yoan, M. Conical Diamond Element PDC Bit as a Breakthrough to Drill Hard Geothermal Formation in Indonesia. In Proceedings of the IADC/SPE Asia Pacific Drilling Technology Conference and Exhibition, Bangkok, Thailand, 27–28 August 2018. [CrossRef]